RSC Advances

PAPER

Cite this: *RSC Adv.*, 2023, **13**, 7554

Cellulose-based sponge@ZIF-8 from waste straws for water disinfection†

Jingyu Li, [ab] Yang Zhang[ab] and Guoxin Sui *[ab]

Received 12th January 2023
Accepted 21st February 2023

DOI: 10.1039/d3ra00243h

rsc.li/rsc-advances

In this study, zeolitic imidazolate framework-8 (ZIF-8) nanoparticles can be readily *in situ* generated on the skeleton surface throughout the entire structure of cellulose-based sponges obtained from waste corn straws *via* a hydrothermal process. Taking natural corn straws as the basic ingredient, the Water Cellulose-based Sponge@ZIF-8 (WCSZ) composite inherits the highly porous structure of straws, which is beneficial for the movement of H_2O molecules in both horizontal and vertical directions. A robust H-bond topological network is weaved between abundant hydroxyl groups of the corn straw cell wall matrix and H_2O molecules in the honeycomb cellular structure. Based on the topological network, the WCSZ composite maintains sufficient mechanical compressibility and elasticity, which could sustain repeated squeezing without structural failure. The WCSZ composite can not only bear a compressive strain as high as 60% but also completely recover its original height after the load is removed, exhibiting excellent mechanical property. More importantly, the WCSZ composite also presents exceptional antibacterial activities after ZIF-8 nanoparticles were introduced (antibacterial rate: 99.9%). Consequently, the WCSZ composite is an ideal candidate for highly efficient elimination of bacteria as the reusable water treatment material.

Introduction

The coexistence of bacteria with other pollutants makes biological decontamination complicated and challenging in natural water environment. Conventional water disinfection technologies including ultraviolet (UV) irradiation activation,[1] chemical inactivation[2] and activated carbon filtration[3] have some serious problems, limiting their further development and practical application. As traditional chemical disinfectants, hypochlorite and chlorine dioxide have been widely applied to treat potable water. However, the disadvantage is the potential production of undesired disinfection by-products such as trihalomethanes and haloacetic acids, which are very harmful for the human body.[4,5] Ultraviolet sterilization may be a useful method, but it lacks sustained effect and will inevitably lead to ozone pollution.[6]

Zeolitic imidazolate frameworks (ZIFs) are the rapidly developing subclass of metal–organic frameworks (MOFs). ZIF-8 is composed of inorganic ligand-transition divalent metal cations and bridging substituted organic ligand-imidazole or imidazole derivative salt anions with zeolite topology.[7] ZIF materials show good performance in the fields of CO_2 capture and storage,[8] gas separation,[9] and heterogeneous catalysis.[10] ZIF-8 nanoparticles are promising functional materials for the modification of the oilfield-produced water treatment antifouling membranes. Halim[11] has developed a nylon 6,6 nanofiber membrane (NFM) incorporating ZIF-8 as the additive for produced water (PW) filtration with more than 80% rejection of oil and excellent suspended solid removal. Recently, we have embarked on studying the possibilities of ZIF-8 as a bactericide for water pollution control. Particularly, ZIF-8 offers us an opportunity to optimize the sterilization performance at the molecular level by rationally tuning metal clusters or organic linkers, which is regarded as a significant competitive advantage of ZIF-8 over traditional bactericides.

The 3D porous materials derived from cellulose have many applications such as hydrogels,[12] aerogels[13] and sensors[14] by virtue of their lightweight structure, biodegradability and sustainability. However, the majority of 3D porous materials derived from cellulose lack adequate mechanical strength, making these materials unsuitable for many applications. Moreover, it is complex to assemble cellulose building blocks into final materials by extracting cellulose from plant cell walls with expensive chemical pretreatments and mechanical disintegration.[15] Throughout history, nature has its way to produce low-density 3D porous materials with exceptional mechanical properties. For example, straws possess three-dimensional interlocked, layered and porous microstructure, featuring mainly vessels and fibers in the longitudinal direction. Their cell walls consist of numerous cellulose nanofibrils and matrix

[a]*Shi-Changxu Innovation Center for Advanced Materials, Institute of Metal Research, Chinese Academy of Sciences, Shenyang 110016, China. E-mail: gxsui@imr.ac.cn*
[b]*School of Materials Science and Engineering, University of Science and Technology of China, Shenyang 110016, China*

† Electronic supplementary information (ESI) available. See DOI: https://doi.org/10.1039/d3ra00243h

components (hemicelluloses and lignin). Moreover, the space between adjacent lamellae is about 50–150 μm, which is in favor of the movement of water molecules in both horizontal and vertical directions. Owing to the aligned and porous structure, straws are endowed with multiple unconventional properties such as energy storage,[16] water treatment[17] and strain sensors.[18] More importantly, cellulose offers a versatile platform for inorganics with controllable structures and tailorable properties because of high surface area, abundant reactive hydroxyl groups and hierarchical structure.[19] Consequently, the biocomposite will present the novel functionalities and performance combined with the hierarchically aligned straw scaffold and inorganic nanoparticles, not known before for cellulosic materials.[20]

In this study, using low-density cellulose-based sponges as the starting material, ZIF-8 nanoparticles can be *in situ* formed on the original honeycomb-like cellular surface of natural cellulose-based straws *via* a hydrothermal process, which enables maximally retaining the intrinsic structure of the straw. As the activator, H_2O molecules are adsorbed and diffused into the honeycomb cellular structure, which will interact with the corn straw cell wall matrix *via* H-bonds. A robust topological network is constructed by a large number of H-bonds attributed to dense intercellulose interactions. The honeycomb-like cellular structure (full of water) is converted into the lamellar structure under compression, which confers sufficient mechanical compressibility and elasticity to the WCSZ composite. Moreover, after being subjected to *E. coli*, the composite displays excellent antibacterial performance. Such mechanically resilient and antibacterial WCSZ composite has great promise for wastewater treatment.

Materials and methods

Materials

Cellulose-based straws with a low density were selected from the same farm (Daqing, Heilongjiang, China). Zinc nitrate hexahydrate ($Zn(NO_3)_2 \cdot 6H_2O$) and ethanol were obtained from Sinopharm Chemical Reagent Co., Ltd, (Shanghai, China). 2-Methylimidazole (2-MeIM), phosphate buffer saline (PBS), and glutaraldehyde solution were provided by Aladdin Biochemical Technology Co., Ltd. (Shanghai). Centrifuge tubes, sterile culture dishes, pipettes and pipette tips, sterile well plates and semipermeable membrane were purchased from Ningbo Zhenhai Hangjing Biotechnology Co., Ltd (Ningbo, Zhejiang, China). Nutrient agar and LB broth were purchased from Qingdao Hope Bio-Technology Co., Ltd (Qingdao, Shandong, China). *E. coli* (ATCC 25922) was provided by Shanghai Lu Wei Technology Co., Ltd. Deionized water was used for all experiments.

Preparation of ZIF-8

ZIF-8 was prepared according to the following synthesis method. The reaction mixture (1 g $Zn(NO_3)_2 \cdot 6H_2O$, 2-MeIM (2.2 g) and 70 mL deionized water) was moved into a steel autoclave (100 mL) and heated at 100 °C for 2 h under magnetic stirring. The resulting white precipitate was collected by repeated centrifugation at 8000 rpm for 30 min, further washed three times with water and methanol, and dried in an oven at 65 °C overnight.

Preparation of water celluose-based sponge@ZIF-8 composites

Fig. 1 shows the schematic of this cellulose-based straw-inspired WSCZ composite. Cellulose-based straws (5 mm × 5 mm × 5 mm) were chosen as the starting material in this experiment. The natural cellulose-based straws were immersed into the solution containing 1 g $Zn(NO_3)_2 \cdot 6H_2O$, 2-MeIM (2.2 g) and 70 mL deionized water. Finally, the reaction mixture was moved into a steel autoclave (100 mL) and heated at 100 °C for 2 h under magnetic stirring. Cellulose-based sponge@ZIF-8 was designed as WCSZ composite. In order to remove the ZIF-8 nanoparticles loosely dispersed on the straw, the fabricated WCSZ composite was washed with deionized water and pressed.

Antibacterial test

In this experiment, *E. coli* was chosen for the antibacterial activity assessment by the zone of inhibition and shaking flask coated plate method. The bacteria were grown in a nutrient broth for 24 h (37 °C) to yield a cell count of approximately 10^9 colony forming units (CFU mL^{-1}). Then bacterial cells were collected by sterile centrifugation and diluted with a sterile PBS solution.

Zone of inhibition:[21] the WCSZ composite and cellulose-based corn straws (control sample) were cut into squares (5 mm × 5 mm × 2 mm). Each sample was put onto the surface of the nutrient agar plate containing about 10^6 CFU mL^{-1} of bacteria and incubated at 37 °C for 24 h, and the size of zone of inhibition was observed.

Shaking flask coated plate method:[21]to determine the anti-*E. coli* activity, 0.5 g cellulose-based corn straw and 0.5 g WCSZ composite were added into the 40 mL sterile 0.01 M PBS water in a conical flask (*E. coli* concentration: 10^5 CFU mL^{-1}), respectively. Then, the conical flask was placed in a constant temperature vibrating incubator at 37 °C for 24 h. The *E. coli* suspensions with 10^5 CFU mL^{-1} concentration were set as the control group. Then, 100 μL of the mixture was taken out from the flask and diluted 10-fold in 24-well plates with PBS at the beginning and the end of the incubation period for 24 h, respectively. Following that, 100 μL of the decimal dilutions were spread on a Petri dish with agar incubated at 37 °C for 24 h. The number of bacterial colonies on each plate was

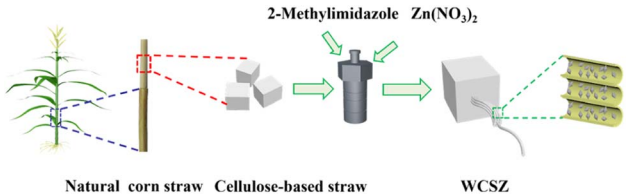

Fig. 1 Schematic of the fabrication of WSCZ composites.

counted. Three parallel experiments were set for each group of experiments. The bacteria after incubating with WCSZ and without WCSZ were observed by SEM. The bacteria were fixed on the samples with 2.5 vol% glutaraldehyde solution for 30 min. Then, the samples were sequentially dehydrated with 15, 30, 50, 70, 90, 95 and 100 vol% ethanol for 20 min, respectively.

$$\text{Killing rate} = \frac{N_c - N_s}{N_c} \times 100\%$$

We marked the amounts of microbial colonies on the plate without WCSZ as N_c, and the amounts of microbial colonies on the plate with WCSZ as N_s.

Characterizations

The morphologies of all the cellulose-based sponge composites and bacteria were observed using an emission scanning electron microscope (SEM, FEI Quanta 400, America) equipped with an energy dispersive X-ray spectroscopic (EDX) detector for mapping. The morphologies of ZIF-8 nanoparticles images were investigated using a transmission electron microscope (TEM, JEM-2100, Japan). The X-ray diffraction (XRD) patterns of samples were measured using a Rigaku Smartlab 9 kW X-ray diffractometer with Cu Kα radiation ($\lambda = 0.154$ nm) in the 2θ range of 5–90° at room temperature. The surface chemical state of samples were investigated by Fourier transform infrared spectroscopy (FTIR, Nicolet 6700, Massachusetts, USA) in the range of 4000–400 cm^{-1}. The density of the dry WCSZ composite was evaluated by weighing the composite and measuring their volumes. The water was then fully filled within the samples. The cyclic compression test with loading–unloading cycles of the WCSZ composite was conducted using a DMA (TA Q700, USA) equipped with a 25 N loading cell at room temperature. The sample (10 mm × 10 mm × 10 mm) of mechanical compressibility was compressed perpendicular to the straw-growth direction with a constant strain rate (5% min^{-1}).

Results and discussion

Every natural corn straw is selected from the same farm in autumn (in November) and the size of the natural straw is selected from the middle part of the natural cellulose-based straw (Fig. 2a). All of the above-mentioned conditions are consistent to ensure the property stability and material consistency of the cellulose-based straw as the natural-resource materials. The natural cellulose-based corn straw with a low density is selected as the starting material to prepare the water cellulose-based sponges. As shown in Fig. 2b, the cellulose-based straw has honeycomb-like cellular structure with thin cell walls and high porosity perpendicular to the straw-growth direction, while vertically aligned fiber tracheids and large-lumen vessels can be clearly seen along the straw-growth direction (Fig. 2c).[22,23] The cellulose cell wall mainly comprises cellulose and vascular bundles, intertwining with each other to provide necessary mechanical integrity to the cellulose-based

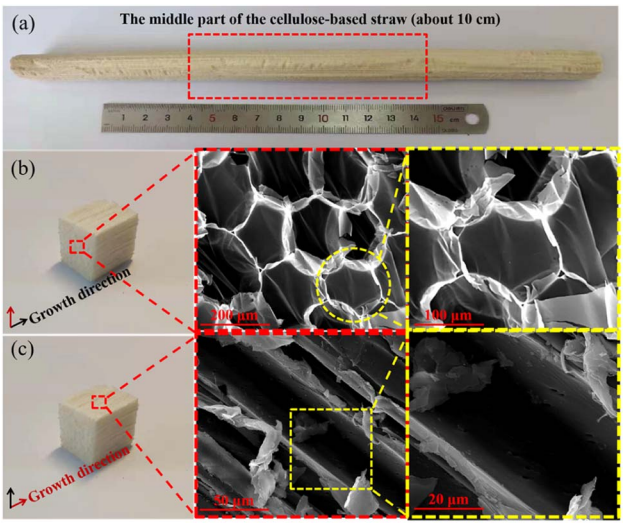

Fig. 2 (a) Photograph of the cellulose-based straw. (b) Photograph of the cellulose-based straw (perpendicular to the straw-growth direction) and its SEM images displaying the honeycomb-like porous structure. (c) Photograph of the cellulose-based straw (along the straw-growth direction) and its SEM images exhibiting the internal structure with exposed cellulose-based straw microfibers.

straw. Such a 3D cellulose-derived scaffold with special structural anisotropy exhibits great potential for further functionalization.

In the natural cellulose-based straw, cellulose fibrils are embedded in a hemicellulose–lignin matrix, providing the straw with the rigidity of cell walls and water stability. The 3D porous cellulose-based straw structure also remains well preserved after *in situ* formation of nanoparticles (Fig. 3a and b). The EDX mapping and elemental analysis (Fig. S1†) further indicate the existence of Zn elements, which are distributed on

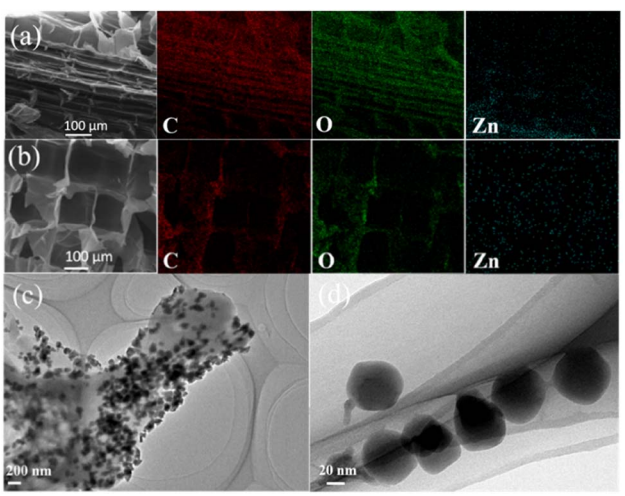

Fig. 3 EDX mappings presenting the elemental distribution of C, O and Zn for (a) dry WCSZ composite along the straw-growth direction and (b) dry WCSZ composite perpendicular to the straw-growth direction. (c and d) TEM images of ZIF-8 on the surface of the corn straw cell wall matrix.

the corn straw cell wall matrix surface. Meanwhile, Fig. 3c and d illustrates the TEM images of ZIF-8 from the WCSZ composite at different magnifications. The corn straw cell wall matrix surface is covered with a substantial number of ZIF-8 nanoparticles (Fig. 3c), which is consistent with the EDX result. The size of ZIF-8 particles (around 60 ± 10 nm in diameter) is gained by 324 particles from Fig. 3c and d.

The X-ray diffraction (XRD) patterns show the characteristic diffraction peaks of the cellulose-based straw corresponding to the 16.8° (110) and 22.5° (200) planes of the native cellulose Iβ (Fig. 4a).[24,25] After the *in situ* growth of ZIF-8 nanoparticles, the dry WCSZ composite shows new characteristic diffraction peaks, consistent with 7.3° (011), 10.4° (002), 12.8° (112) and 18.1 (222) planes of pure ZIF-8 nanoparticles (Fig. 4b and c),[26] compared with the natural cellulose-based straw.

The characteristic peaks for ZIF-8 and cellulose can be seen in the FTIR results of WSCZ (Fig. S2a†). From Fig. S2b,† it can be observed that the absorption peak at 3138 cm^{-1} is attributed to the stretching vibration of the C–H bond. The peak at 2933 cm^{-1} is attributed to imidazole rings, the peak at 1580 cm^{-1} is related to the C=N stretching vibration and the peak at 990 cm^{-1} is assigned to the C–N stretching vibration.[27] The FTIR result of the cellulose-based straw is shown in Fig. S2c;† the bands related to the pyranose ring stretching vibration (1109 and 1041 cm^{-1}) are from cellulose.[28]

FTIR spectroscopy was employed to understand the H-bond interactions between adjacent WSCZ chains. For instance, the cellulose-based straw shows a peak for –OH at 3338 cm^{-1} as a result of extensive H-bond interactions, whereas after the *in situ* growth of ZIF-8, the absorption peak increases to 3345 cm^{-1}, and a blueshift of 7 cm^{-1} was observed as compared with the cellulose-based straw.

The mechanical compressibility of the WCSZ composite perpendicular to the vascular bundle direction is demonstrated in Fig. 5a. The compressive stress as a function of strain was measured to assess the mechanical properties of the WCSZ composite. Under maximum compressive strains (20, 40 and 60%), the compressive stress–strain curves of the WCSZ composite are presented in Fig. 5b. The WCSZ composite can not only bear a compressive strain as high as 60% but also completely recover its original height after the load is removed, exhibiting excellent mechanical property compliance in sharp contrast to the cellulose-based straw without water (Fig. S3a–d†). The cellulose-based straw without water exhibits its irreversible compressibility with substantial plastic deformation. As the activator, the water molecules themselves are firmly held in place in the 3D hierarchical hollow fibers with cell walls. A topological network is weaved between H_2O molecules and cellulose macromolecules *via* H-bonds in the honeycomb structure.[29]

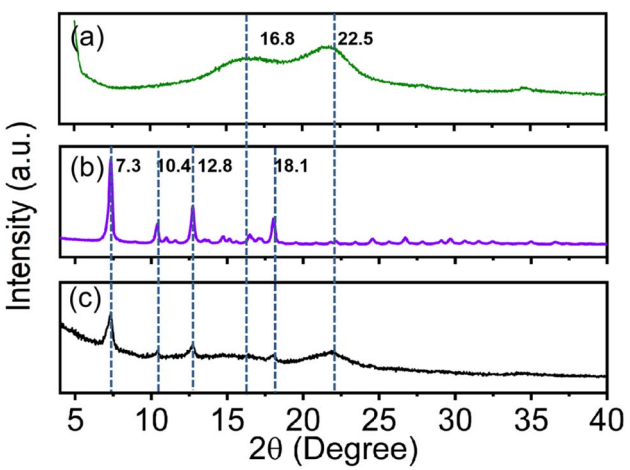

Fig. 4 XRD patterns of (a) corn straw, (b) ZIF-8 and (c) WCSZ.

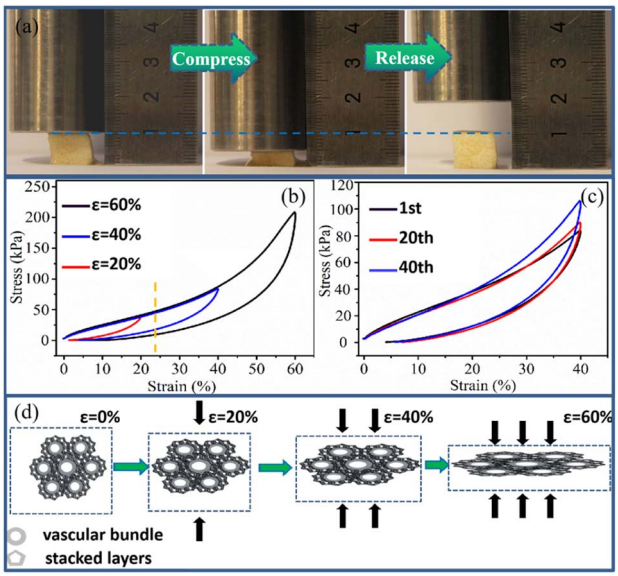

Fig. 5 (a) Photographs of the WCSZ composite exhibiting the reversible compressibility perpendicular to the vascular bundle direction. (b) Compression stress–strain curves of the WCSZ composite under maximum strains (20, 40 and 60%). (c) Compression stress–strain curves of the WCSZ composite under successive compression at the maximum strain (40%). (d) Schematic of the compressibility deformation behavior of the WCSZ composite perpendicular to the vascular bundle direction.

There are two distinct regions under compression, involving a linear elastic region (~20%) strain and a subsequent densification region, where the stress increases sharply with the strain. The initial linear elastic region originated from the elastic deformation of stacked layers in the WCSZ composite. Then, as the support structure, vascular bundles play a crucial role in the subsequent densification region during loading of samples. The compressive stress–strain curve of the WCSZ composite can be explained by the deformation behavior of cells (Fig. 5d). From the 0–20% strain, it is the elastic region where the stacked layers associate with the support part elastically *via* compact H-bonds. With the increase in strain, sliding and bending of cell walls occur in response to the compressive loading. The honeycomb-like cellular structure of the WCSZ composite is converted into the lamellar structure upon proper stress, absorbing much more energy (20–60% strain). The topological network allows for load transfer between cellulose

skeletons by bending and bucking of the WCSZ composite.[30] Importantly, though the edges of cell walls broke, the center of the cell walls remains intact, such that the sample can recover to its original shape after the release of stress. A cyclic loading–unloading compression test was performed on the WCSZ composite at a constant strain (40%) (Fig. 5c). Interestingly, the compressive strength of WCSZ is increased from 84 kPa (first time) to 106 kPa (40th time) with continuous compression. This is attributed to the water loss (gravity and pressing) in the test that results in the densification of the WCSZ composite associated with height decrease in the compress release cycles. Finally, we selected a wide range of 3D porous materials based on cellulose reported in the literature[31–36] and compared their maximum compressive strength with the WCSZ composite. The maximum compressive strength of the WCSZ composite is higher than that of the other materials made from cellulose materials (Table 1).

Considering that the water environment can induce the growth of bacteria,[37] the WCSZ composite with bacteriostatic effects can be a promising candidate for practical applications by virtue of its high porosity[38] and mechanical flexibility. In this experiment, we chose *Escherichia coli* (*E. coli*) as a representative bacterium to evaluate the bacteriostatic performance. The antibacterial activity of the WCSZ composite against *E. coli* was determined by a spread plate method (Fig. 6a and b). As a control sample, the agar medium containing the cellulose-based corn straw was fully covered with bacteria, suggesting that the natural cellulose-based straw does not show any antibacterial activity by itself. By contrast, the agar medium covered with WSCZ exhibits obvious inhibition zones against *E. coli*;[39,40] in other words, WCSZ shows much better antibacterial activities than those of the natural cellulose-based straw. The result indicated that the remarkable bacteriostatic activity came from the release of Zn^{2+} ions of ZIF-8 nanoparticles, which is a major mechanism for oligodynamic activities against eukaryotic and prokaryotic microorganisms.[41] *E. coli* adsorbed on the natural cellulose-based straw display intact membranes and smooth surface (1000 nm in length and 500 nm in width) (Fig. 6c–e). By contrast, when *E. coli* are attached on the surface of the WCSZ composite, it shows various degrees of deformation such as wrinkles and even cracks, implying that Zn^{2+} released from the WCSZ composite contributes to the destruction of the cell membranes and further cytoplasm leakage of *E. coli* (Fig. 6f–h).

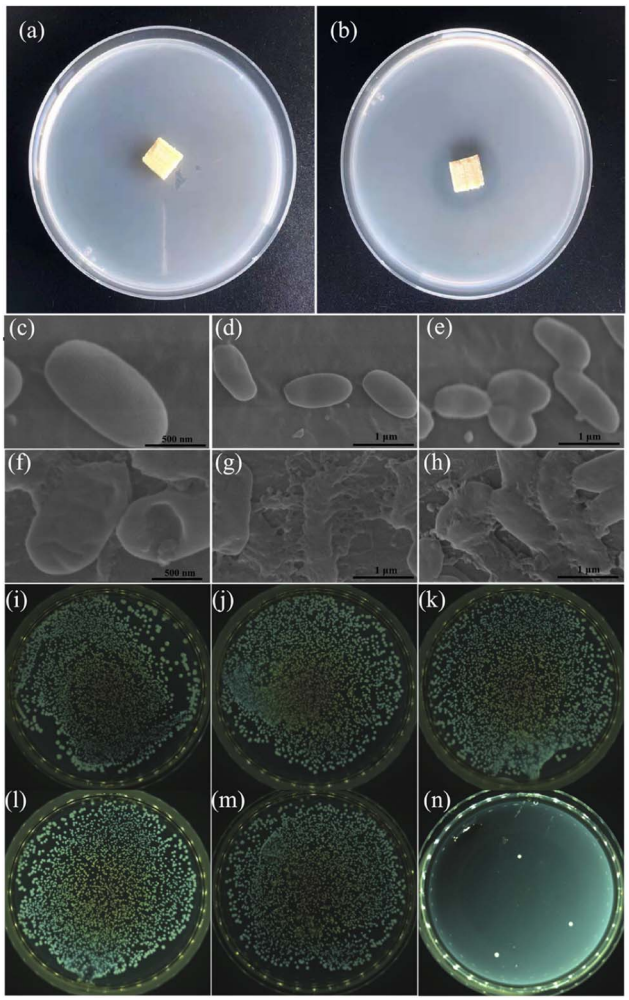

Fig. 6 Photographs of *E. coli* incubated on agar plates with (a) natural corn straw and (b) with WCSZ composite. SEM images of *E. coli* in touch (c–e) with natural corn straw and (f–h) with WCSZ composite. Photographs of colonies of *E. coli* incubated on agar plates with (i) blank, (j) natural cellulose-based straw, and (k) WSCZ for 0 h. Photographs of colonies of *E. coli* incubated on agar plates with (l) blank, (m) natural cellulose-based straw, and (n) WSCZ for 24 h.

The WCSZ composite exhibits excellent antibacterial activities (antibacterial rate: 99.9%). The number of colonies of *E. coli* incubated on agar plates with blank, natural cellulose-based straw, and WSCZ for 0 h is 2265, 2232 and 2562, respectively

Table 1 Maximum compressive strength of the WSCZ composite compared with various 3D porous materials obtained from cellulose

Year	3D porous materials	Density (mg cm^{-3})	Compressive strength (kPa)	Ref.
2014	Silylated cellulose sponge	6.7–17.3	6	35
2018	Silylated wood sponge	30.1	25	32
2019	Silylated aerogel	5.7–10.95	46	36
2010	Carbon nanofiber aerogel	5.6	60	31
2020	Cellulose nanocrystal-based aerogel	18.6	90	34
2017	Biomass-derived aerogel	52	120	33
2023	Water cellulose sponge@ZIF-8	32.2	200	This work

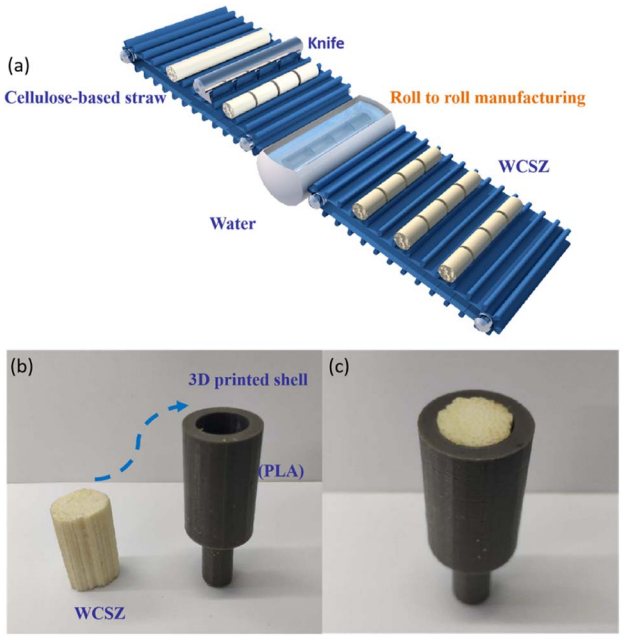

Fig. 7 (a) Schematic displaying the roll-to-roll manufacture of the WCSZ composite. (b and c) Photographs of the potential application of the WCSZ composite as a portable device combined with polymer shells (3D printing).

(Fig. 6i–k). While the number of colonies of *E. coli* incubated on agar plates with blank, natural cellulose-based straw, and WSCZ for 24 h is 2571, 2567, 3, respectively (Fig. 6l–n). The results indicate that the pure natural cellulose-based straw does not have anti-*E. coli* ability and the WSCZ composite has potential application in the field of anti-*E. coli*.

Using established techniques (roll-to-roll), the WCSZ composite manufacture process can be made scalable by infiltration and hydrothermal methods, as shown in Fig. 7a. As the resilient and sustainable resource, the WCSZ composite has the potential application as portable devices for water treatment, in which water transports along the straw-growth direction. For example, an integrated WCSZ composite can be successfully applied to polymer shells combined with 3D printing technology, and the resulting integrated WCSZ composite as a novel "cross-flow" filtration device shows high flexibility to accommodate the polymer shell (Fig. 7b and c).

Conclusions

In summary, ZIF-8 nanoparticles can be readily *in situ* generated on the skeleton surface throughout the entire structure of cellulose-based sponges obtained from waste corn straws *via* a hydrothermal process. Taking reproducible natural corn straws as the basic ingredient, the WCSZ composite inherits the highly porous structure of straw. The WCSZ composite can not only bear a compressive strain as high as 60% but also completely recover its original height after the load is removed, exhibiting excellent mechanical property. More importantly, the WCSZ composite also presents exceptional antibacterial activities (antibacterial rate: 99.9%) after the ZIF-8 nanoparticles were introduced. Consequently, the WCSZ composite is an ideal candidate for highly efficient elimination of bacteria as the reproducible water treatment material. The facile and low-cost approach may shed light on the design for cellulose scaffolds with special functionalities directly from the natural cellulose-based straw.

Author contributions

Jingyu Li: conceptualization, investigation, project administration, formal analysis, software, methodology, data curation, writing-original draft. Yang Zhang: investigation, writing-original draft. Guoxin Sui: conceptualization, supervision, project administration, formal analysis, data curation, writing-review & editing, funding acquisition.

Conflicts of interest

The authors declare that they have no known competing financial interests or personal relationships that could have appeared to influence the work reported in this paper.

Acknowledgements

This research received no external funding.

References

1 L. Tasic, D. Stanisic, C. H. N. Barros, L. K. Covesi and E. R. Bandala, *Catalysts*, 2022, **12**, 430.
2 M. Jütte, J. V. Große, M. S. Abdighahroudi, C. Schüth and H. V. Lutze, *Environ. Sci.: Water Res. Technol.*, 2022, **8**, 630–639.
3 C. M. Klevens, M. R. Collins, R. Negm, M. F. Farrar and R. Mastronardi, *ACS Symp. Ser.*, 1996, **649**, 211–250.
4 Y. Wang, A. Jia, Y. Wu, C. Wu and L. Chen, *Environ. Technol.*, 2015, **36**, 479–486.
5 H. W. Levitin, H. J. Siegelson, S. Dickinson, P. Halpern and D. Turineck, *Prehosp. Disaster Med.*, 2003, **18**, 200–207.
6 H. Fleming and W. Huebner, *Water Eng. Manage.*, 2001, **148**, 13–16.
7 J. J. DelgadoMarin, D. P. Izan, M. Molina-Sabio, E. V. Ramos-Fernandez and J. Narciso, *Molecules*, 2022, **27**, 1968.
8 F. Yang, T. Ge, X. Zhu, J. Wu and R. Wang, *Sep. Purif. Technol.*, 2022, **339**, 117090.
9 M. E. Casco, Y. Q. Cheng, L. L. Daemen, D. Fairen-Jimenez, E. V. Ramos-Fernandez, A. J. Ramirez-Cuesta and J. Silvestre-Albero, *Chem. Commun.*, 2016, **52**, 3639–3642.
10 M. A. Rivero-crespo, M. Mon, M. A. Rivero-Crespo, J. Ferrando-Soria, C. W. Lopes, M. Boronat, A. Leyva-Pérez, A. Corma, J. C. Hernández-Garrido, M. López-Haro, J. J. Calvino, E. V. Ramos-Fernandez, D. Armentano and E. Pardo, *Angew. Chem., Int. Ed. Engl.*, 2018, **57**, 17094–17099.
11 N. S. A. Halim, M. D. H. Wirzal, M. R. Bilad, N. A. H. Md Nordin, Z. Adi Putra, A. R. Mohd Yusoff, T. Narkkun and K. Faungnawakij, *Water*, 2019, **11**, 2111.

12 K. S. M. Fijul, P. P. Sikdar, B. Haque, B. M. A. Rahman, A. Ali and M. N. Islam, *Prog. Biomater.*, 2018, **7**, 153–174.
13 S. T. Nguyen, J. Feng, N. T. Le, A. Le, N. Hoang, V. Tan and H. M. Duong, *Ind. Eng. Chem. Res.*, 2013, **52**, 18386–18391.
14 S. Ummartyotin and H. Manuspiya, *Renewable Sustainable Energy Rev.*, 2015, **41**, 402–412.
15 X. Li, X. Lu, J. Yang, Z. Ju, Y. Kang, J. Xu and S. Zhang, *Green Chem.*, 2019, **21**, 2699–2708.
16 Z. Gui, H. Zhu, E. Gillette, X. Han, G. W. Rubloff, L. Hu and S. B. Lee, *ACS Nano*, 2013, **7**, 6037–6046.
17 W. Chao, S. Wang, Y. Li, G. Cao and S. Ho, *Chem. Eng. J.*, 2020, **400**, 125865.
18 H. Liu, H. Jiang, F. Du, D. Zhang, Z. Li and H. Zhou, *ACS Sustainable Chem. Eng.*, 2017, **5**, 10538–10543.
19 N. Sun, Z. Li, X. Zhang, W. Qin, C. Zhao, H. Zhang, D. H. L. Ng, S. Kang, H. Zhao and G. Wang, *ACS Sustainable Chem. Eng.*, 2019, **7**, 8735–8743.
20 Y. Shchipunov and I. Postnova, *Adv. Funct. Mater.*, 2018, **28**, 1705042.
21 J. Li, J. Li, J. Wei, X. Zhu, S. Qiu and H. Zhao, *ACS Appl. Mater. Interfaces*, 2021, **13**, 10446–10456.
22 J. Song, C. Chen, S. Zhu, M. Zhu, J. Dai, U. Ray, Y. Li, Y. Kuang, Y. Li, N. Quispe, Y. Yao, A. Gong, U. H. Leiste, H. A. Bruck, J. Y. Zhu, A. Vellore, H. Li, M. L. Minus, Z. Jia, A. Martini, T. Li and L. Hu, *Nature*, 2018, **554**, 224–228.
23 G. Chen, T. Li, C. Chen, C. Wang, Y. Liu, W. Kong, D. Liu, B. Jiang, S. He, Y. Kuang and L. Hu, *Adv. Funct. Mater.*, 2019, **29**, 1902772.
24 H. O. M. Moura, L. M. A. Campos, V. L. D. Silva, J. C. F. D. Andrade, S. M. N. D. Assumpção, L. A. M. Pontes and L. S. D. Carvalho, *Cellulose*, 2018, **25**, 5669–5685.
25 A. D. French, *Cellulose*, 2014, **21**, 885–896.
26 X. Fan, W. Wang, W. Li, J. Zhou, B. Wang, J. Zheng and X. Li, *ACS Appl. Mater. Interfaces*, 2014, **6**, 14994–14999.
27 J. A. Schott, C. Do-Thanh, W. Shan, N. G. Puskar, S. Dai and S. M. Mahurin, *Green Chem. Eng.*, 2021, **2**, 392–401.
28 C. Yang, X. Lu, W. Lin, X. Yang and J. Yao, *Chem. Res. Chin. Univ.*, 2006, **22**, 524–532.
29 D. Zhao, Y. Zhu, W. Cheng, G. Xu and L. Hu, *Matter*, 2019, **2**, 390–403.
30 X. Han, T. Wang, P. S. Owuor, S. H. Hwang, C. Wang, J. Sha, L. Shen, J. Yoon, W. Wang, R. V. Salvatierra, P. M. Ajayan, R. Shahsavari, J. Lou, Y. Zhao and J. M. Tour, *ACS Nano*, 2018, **12**, 11219–11228.
31 X. Gui, J. Wei, K. Wang, A. Cao, H. Zhu, J. Yi, Q. Shu and D. Wu, *Adv. Mater.*, 2010, **22**, 617–621.
32 H. Guan, Z. Cheng and X. Wang, *ACS Nano*, 2018, **12**, 10365–10373.
33 J. Jiang, Q. Zhang, X. Zhan and F. Chen, *ACS Sustainable Chem. Eng.*, 2017, **5**, 10307–10316.
34 D. Li, Y. Wang, F. Long, L. Gan and J. Huang, *ACS Appl. Mater. Interfaces*, 2020, **12**, 1549–1557.
35 Z. Zheng, G. Sèbe, D. Rentsch, T. Zimmermann and P. Tingaut, *Chem. Mater.*, 2014, **26**, 2659–2668.
36 X. Zhang, M. Liu, H. Wang, N. Yan, Z. Cai and Y. Yu, *Carbohydr. Polym.*, 2019, **208**, 232–240.
37 D. Ma, P. Li, X. Duan, J. Li, P. Shao, Z. Lang, L. Bao, Y. Zhang, Z. Lin and B. Wang, *Angew. Chem.*, 2020, **132**, 3933–3937.
38 S. He, C. Chen, G. Chen, F. Chen and L. Hu, *Chem. Mater.*, 2020, **32**, 1887–1895.
39 S. Y. H. Abdalkarim, H. Yu, M. Song, Y. Zhou, J. Yao and Q. Ni, *Carbohydr. Polym.*, 2017, **176**, 38–49.
40 S. Thambidurai, P. Gowthaman, M. Venkatachalam and S. Suresh, *J. Alloys Compd.*, 2020, **830**, 154642.
41 J. Li, Y. Zhang, H. Zhao and G. Sui, *Nanomaterials*, 2023, **13**, 202.